NANO LETTERS

Letter

pubs.acs.org/NanoLett

Efficient Production of Single-Stranded Phage DNA as Scaffolds for DNA Origami

Benjamin Kick,[†] Florian Praetorius,[‡] Hendrik Dietz,[‡] and Dirk Weuster-Botz*,[†]

[†]Institute of Biochemical Engineering, Technische Universität München, Boltzmannstr. 15, 85748 Garching, Germany

[‡]Physik Department, Walter Schottky Institute, Technische Universität München, Am Coulombwall 4a, 85748 Garching, Germany

Supporting Information

ABSTRACT: Scaffolded DNA origami enables the fabrication of a variety of complex nanostructures that promise utility in diverse fields of application, ranging from biosensing over advanced therapeutics to metamaterials. The broad applicability of DNA origami as a material beyond the level of proof-of-concept studies critically depends, among other factors, on the availability of large amounts of pure single-stranded scaffold DNA. Here, we present a method for the efficient production of M13 bacteriophage-derived genomic DNA using high-cell-density fermentation of *Escherichia coli* in stirred-tank bioreactors. We achieve phage titers of up to 1.6×10^{14} plaque-forming units per mL. Downstream processing yields up to 410 mg of high-quality single-stranded DNA per one liter reaction volume, thus upgrading DNA origami-based nanotechnology from the milligram to the gram scale.

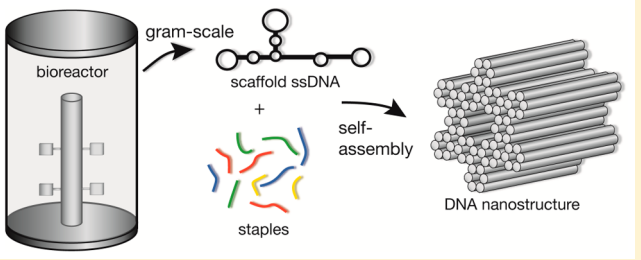

KEYWORDS: *DNA origami, single-stranded DNA, bacteriophage M13, high-cell-density fermentation, self-assembly*

Scaffolded DNA origami is a versatile bottom-up method for the production of three-dimensional nanostructures that entails folding of long, single-stranded scaffold DNA molecules guided by sets of short single-stranded DNA.[1−3] DNA origami objects have been developed as nanotools in various fields of applications, including—but not limited to—NMR spectroscopy,[4,5] single-molecule sensing,[6−11] plasmonics,[12] and cell biology.[13] Furthermore, several DNA origami-based drug-delivery systems have been proposed.[14−17]

To advance from the level of proof-of-concept studies, many applications ultimately require gram-scale amounts of DNA objects. While significant progress has been made with respect to optimizing synthesis yields and object purification,[18−20] the availability of the raw materials ultimately limits the amount of DNA origami objects that can be produced.

A variety of enzymatic methods enable the production of single-stranded DNA (ssDNA), for example asymmetric polymerase chain reaction (PCR),[21] separation of a biotinylated strand using streptavidin beads,[22] lambda nuclease digestion of one phosphorylated strand,[23,24] size separation of length modified strands in urea-denaturing polyacrylamide gel electrophoresis,[25,26] rolling circle amplification of a circular template,[27−31] or nicking and subsequent digestion of one strand of a plasmid.[2] All of these methods use purified enzymes or deoxynucleotides or both, and the synthesis of ssDNA using these methods tends to be practically limited to the μg−mg scale.

An alternative and more scalable solution for ssDNA production makes use of bacteriophages with fast growing *Escherichia coli* (*E. coli*) cells as host. The filamentous, nonlytic bacteriophage M13 is composed of a circular ssDNA genome coding for 11 viral proteins enveloped by a protein coat. Progeny phage particles are assembled during secretion of intracellularly amplified viral ssDNA without lysis of the host. These viable host cells are able to divide beyond infection. Variants of the ssDNA genome of bacteriophage M13mp18 are commonly used as scaffold material for DNA origami objects. So far, scaffold production with bacteriophages has been performed with simple batch-processes on a shake flask scale with reported yields ranging from 1 to 14 mg of purified ssDNA per liter culture.[32,33] In our experience, this method reproducibly yields approximately 4 mg of purified ssDNA per one liter of fermentation volume. Hence, producing a mere gram of scaffold DNA using shaker cultures appears very difficult, because of the sheer volume of culture that would need to be processed.

To achieve a scalable and efficient ssDNA production process, we have thus developed a high-cell-density fermentation of bacteriophage-infected *E. coli* in a stirred-tank bioreactor under controlled pH, dissolved oxygen and substrate supply conditions that yield gram-scale amounts of purified ssDNA.

A high-cell-density fermentation process was established with *E. coli* growing without phage infection as reference in a fully controlled lab-scale stirred-tank bioreactor up to a biomass concentration of 94 ± 2 g L^{-1} cell dry weight within 45 h (Figure 1), corresponding to an optical density of 213 ± 3 at

Received: April 15, 2015
Revised: May 28, 2015
Published: June 1, 2015

DOI: 10.1021/acs.nanolett.5b01461
Nano Lett. 2015, 15, 4672−4676

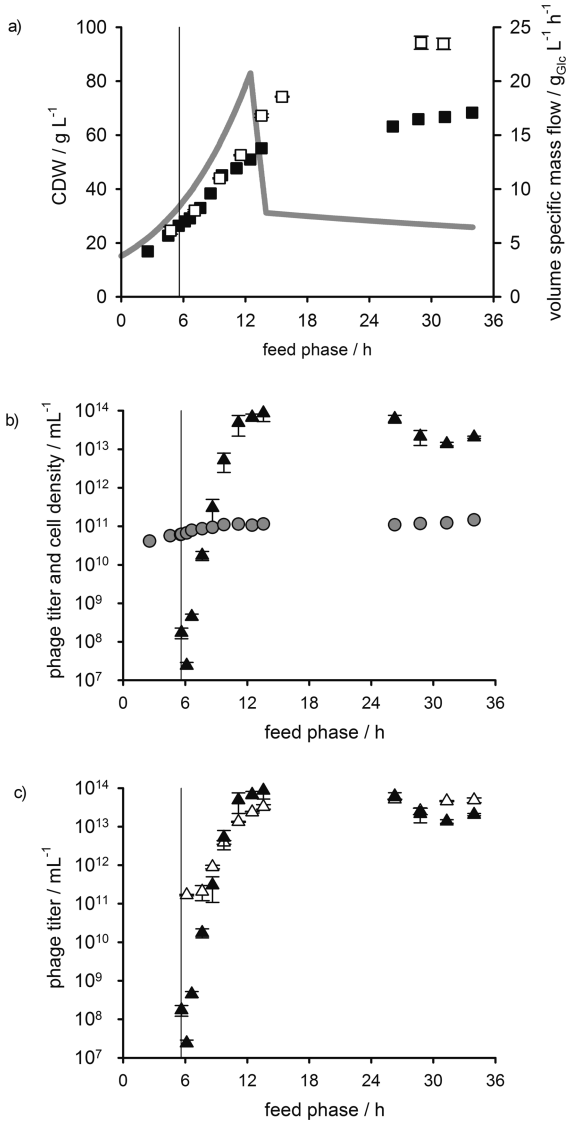

Figure 1. Bacteriophage M13 infection during a high-cell-density fermentation of *E. coli* in a lab-scale stirred-tank bioreactor. Vertical line indicates time of phage infection in feed phase. (a) Cell dry weight (CDW) of *E. coli* XL1-blue MRF' with (■) and without (□) phage infection; volume specific feed profile of glucose (gray line). (b) Comparison of phage titer (▲) analyzed with plaque assay and host cell density (gray circle). (c) Quantification of phage titer with plaque assay (▲) and absorbance at 269 nm (white triangle).

600 nm.[34,35] After the initial batch phase the cell specific growth rate was controlled to 0.15 h^{-1} through glucose-limited exponential feeding. After 12 h of exponential feeding the substrate supply rate was decreased linearly within 1.5 h until 7.7 g_{Glc} L^{-1} h^{-1} to avoid oxygen limitation. This flow rate was kept constant until the end of the process.

In a second fermentation process with identical reaction conditions, growing host cells were infected with M13 bacteriophages after 5.6 h of glucose feeding. Until 6 h after infection no significant difference regarding cell dry weight concentrations and growth rate were observed between infected or uninfected cells (Figure 1a). The final maximum cell dry weight concentration was 28% lower than in the reference process without phage infection. The phage titer dropped down directly after infection due to the fast infection of host cells after addition of bacteriophages M13 (4 min after addition of phage ssDNA is produced intracellularly).[36] Within 8 h after infection the phage titer increased by a factor of 10^6 and reached $8.7 \pm 3.4 \times 10^{13}$ pfu mL^{-1} (pfu = plaque forming unit) (Figure 1b). The ratio between phage and host cell increased after infection from 0.002 up to 1000 pfu cfu^{-1} (Figure 2c).

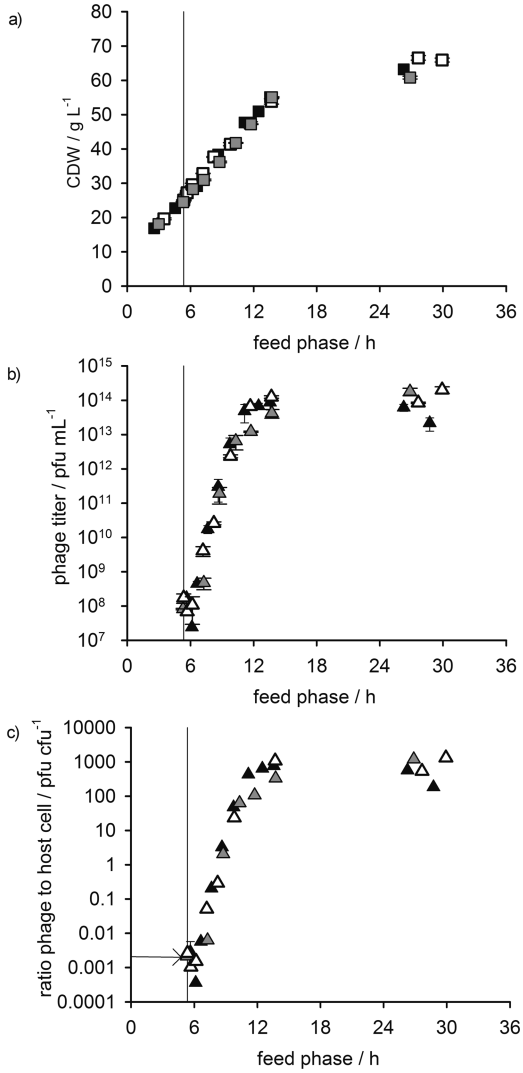

Figure 2. Phage production with different ssDNA genome length. Fed-batch fermentation of *E. coli* in a lab-scale stirred-tank bioreactor with three phage variants with 7249 (white), 7560 (black) and 8064 bases (gray). Vertical line indicates time of phage infection in feed phase. (a) Cell dry weight of *E. coli* XL1-blue MRF′. (b) Phage titer analyzed with plaque assay. (c) Ratio between phages and host cells during feed phase; arrow indicates the multiplicity of infection of 0.002.

Phage quantification using absorbance measurements at 269 nm was applied to verify the data derived from the plaque assay (Figure 1c).[37] The plaque assay is shown to be the quantification method of choice below 10^{11} pfu mL^{-1} although it is laborious and time-consuming. At higher phage concentrations the two methods are in good agreement, especially at the end of the process, where the quantification at 269 nm revealed lower variations than the plaque assay.

In batch experiments under unlimited substrate concentrations, an infection with nonlytic bacteriophage M13 reduces the maximum growth rate of host cells.[32] A maximum growth rate of 0.33 h^{-1} with the *E. coli* XL1-blue MRF′ strain was

DOI: 10.1021/acs.nanolett.5b01461
Nano Lett. 2015, 15, 4672−4676

observed in defined salt medium in batch fermentations, which is consistent with published data using the same medium and strain. The low maximum growth rate is due to a point mutation (E115 K) in *purB* gene, coding for adenylosuccinate lyase.[38] The maximum growth rate of infected host cells was reduced to 0.24 h^{-1} in batch fermentation in stirred-tank reactors under comparable conditions regarding temperature, pH and dissolved oxygen concentration. Although phage infection reduces maximal growth rate, a predefined exponential feeding with a specific growth rate of 0.15 h^{-1} led to no difference of growth comparing infected and uninfected host-cell in the first 6 h after infection. The difference in cell dry weight at the end of the fed-batch process could be explained by the high phage titer in comparison to the host cell density and the influence of phage infection on transcription, translation and metabolic pathways.

Up to now titers of filamentous phages in stirred-tank batch experiments were reported to reach 1.2×10^{11} pfu mL^{-1}[39] and 3.5×10^{11} pfu mL^{-1}.[40] An improved method for M13 phage fermentation in shake flasks gave titers of up to 10^{12} pfu mL^{-1},[41] whereas Hofschneider reported a bacteriophage M13 titer of 3×10^{12} pfu mL^{-1} in 1963.[42] Thus, the M13 phage titer of $1.6 \pm 0.4 \times 10^{14}$ pfu mL^{-1} achieved in the high-cell-density fed-batch process represents a 50-fold increase compared to literature. Furthermore, in contrary to literature we demonstrate that high phage titers at high host cell densities do not exclude each other.[39]

For the scaffolded DNA origami method a set of scaffold DNA variants are in use, based on the M13mp18 (7249 b) backbone, for example variants with 7560 and 8064 bases.[2] The variants led to a higher degree of freedom in design of DNA origami objects. With the demand for different ssDNA variants the question arose whether length modifications in the multiple cloning site of the M13 genome have an effect on the process performance for phage production. High-cell-density fermentations with different phage variants resulted in reproducible results if time of infection and multiplicity of infection was kept constant (Figure 2). The multiplicity of infection (in our case MOI = 0.002 pfu cfu^{-1}) describes the ratio between phage particles to host cells at time of infection.

Maximum phage titers and phage amplification rates were reproduced in high-cell-density fed-batch processes for the different phage variants. The stagnation in phage titer at the end of the production process remains an open question and will be investigated in future.

After liquid–solid separation (centrifugation) of host cells and extracellular bacteriophages at the end of each fed-batch process, the phages are precipitated using polyethylene glycol 8000.[43,44] The protein coat is chemically lysed while the ssDNA is purified by ethanol precipitation (see Supporting Information for details). Up to 0.41 g of purified ssDNA was obtained from one liter fermentation broth (Table 1). The overall yield of the downstream process varied between 50 and 60%, assuming one phage particle relates to one ssDNA molecule. Beneath the phage production process, the downstream process and ssDNA yield indicates a reproducible production process for ssDNA.

Table 1. Produced Amount and Overall Yield of Different ssDNA Variants

ssDNA	yield (%)	isolated ssDNA, g per L reaction volume
7249 b	55	0.41 ± 0.01
7560 b	60	0.37 ± 0.04
8064 b	50	0.37 ± 0.01

To analyze the purity and integrity of the thus produced ssDNA, we compared it to ssDNA from two commercial vendors and to ssDNA prepared from shaker flask cultures (Figure 3).

Electrophoretic mobility analysis of the different ssDNA samples on agarose gels showed comparable band patterns. The absence of additional bands points against the occurrence of a potentially elevated content of degraded ssDNA products for our bioreactor-based ssDNA (Figure 3 a). We used the same set of ssDNA samples to fold a variant of Rothemund's single layer DNA rectangle [1] (Figure 3 b and c) and three different multilayer DNA origami structures[46,47,20] (Figure 3 c and d). Our rectangle variant contains a single-stranded adaptable loop that can accommodate the genomic insert. This insert discriminates the three different scaffold lengths. Hence, the rectangle variant can be assembled with each of the scaffold variants. An electrophoretic mobility analysis on agarose gels of products in folding reaction mixtures of this rectangle revealed comparable band patterns for the scaffolds of different origins. Importantly, due to the longer single-stranded scaffold loop structures folded with longer scaffolds migrate more slowly in the gel. Previous publications suggest that incubation of phage-infected cultures for over 5 h may lead to deletion of the insert and consequential shortening of the ssDNA.[32] However, the absence of a faster band in the lanes containing 7560 or 8064 base variants shows that these rearrangements do not occur in the bioreactor produced samples (Figure 3b). Folding of more complex multilayer DNA origami structures did not show any differences between the different scaffolds (Figure 3d). Well-folding structures like the pointer and the 42-helix bundle objects show no additional bands or impurities when using the bioreactor-based scaffold DNA. The gear-like object sample is a design that features a greater propensity to form side products and aggregates during self-assembly as compared to the other structures. Nonetheless, reaction products for this more sensitive design also show comparable migration behavior, regardless of the origin of the scaffold used. We thus conclude that the method we present here allows us to produce large quantities of scaffold DNA that has comparable quality to the scaffold DNA produced from the conventional, low yield methods.

Conclusion. Taken together, the transfer of bacteriophage production from shake flasks to high-cell-density fermentation in a stirred-tank bioreactor allowed us to achieve a fifty-fold increase in maximal phage titer, which enables a process for the efficient production of single-stranded DNA on the gram scale per liter-reaction-volume, thus increasing the efficacy of scaffold DNA production by 2 orders of magnitude compared to previous methods.[32,42] As a consequence the synthesis of long ssDNA scaffolds is no longer a limiting factor in the production of large amounts of DNA origami objects. Important challenges for the future include addressing the availability of large amounts of short single-stranded DNA oligonucleotides with custom sequences, which are nowadays typically synthesized via chemical solid-phase synthesis. Recently, a phagemid system relying on helper phage rescue and enzymatic digestion has been successfully used to produce staple strands for DNA origami.[28] The combination of this technique with the process presented here could facilitate the biotechnological production of single-stranded DNA oligonucleotides on a gram scale.

DOI: 10.1021/acs.nanolett.5b01461
Nano Lett. 2015, 15, 4672–4676

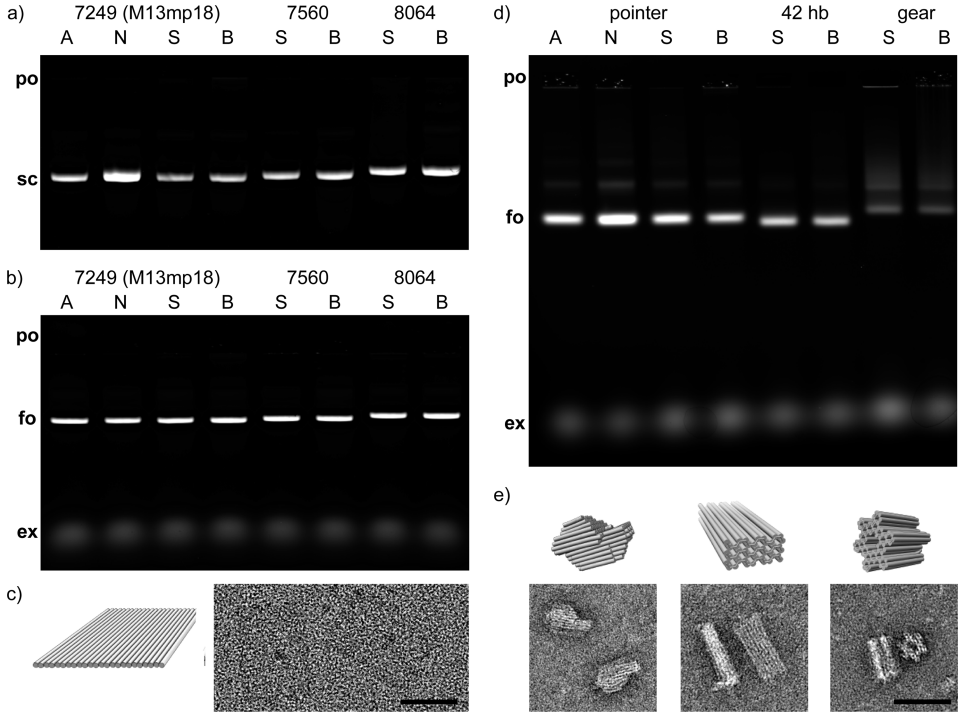

Figure 3. Evaluation of purity and integrity of scaffold ssDNA. (a) Image of an agarose gel on which scaffold strands of different lengths (7249, 7560, and 8064 bases) prepared with different methods were electrophoresed. Labels: A, Affymetrix; N, New England Biolabs (both commercial vendors); S, shaker flask; B, bioreactor; po, pocket; sc, scaffold band. (b) Image of a gel on which products from self-assembly reaction mixtures for a variant of Rothemund's single layer rectangle[1] were electrophoresed, using the scaffold DNA samples from (a). Additional labels: fo, folded structures; ex, excess staples. (c) Illustration (left) and TEM micrograph of a Rothemund rectangle variant folded with 7249 b scaffold prepared from controlled fed-batch process in bioreactor. Scale bar: 50 nm. (d) Image of a gel on which products from self-assembly mixtures of three different multilayer structures folded with the scaffolds from (a) were electrophoresed. The pointer uses 7249-, the 42-helix bundle uses 7560-, and the gear uses 8064 bases long scaffold. (e) CanDo-computed[3,45] models (top) and negative-stain TEM micrographs (bottom) of the three structures from (d). Scale bar: 50 nm.

Material and Methods. Controlled fed-batch processes were performed with a stirred-tank bioreactor system (KLF Advanced System 3.6 L, Bioengineering AG, Wald, Switzerland) with a batch volume of 1.6 L of Riesenberg basal medium adding 25 g L^{-1} glucose, 1 mM thiamin-HCl, and 50 mg L^{-1} Kanamycin A.[34] For inoculation of the bioreactor, the exponential growing cells in shake flasks were concentrated 10 min at 20 °C, 3260 rcf, and resuspended in 20 mL of Riesenberg basal medium to get a defined starting cell mass. The feed phase started after the depletion of batch glucose and consequent rise of dissolved oxygen concentration with the profile shown in Figure 1a (see Supporting Information for feed profile equation); feed solution consists of 750 g L^{-1} glucose, 20 g L^{-1} $MgSO_4 \times 7$ H_2O and 18.5 g L^{-1} $(NH_4)_2SO_4$. All components of the feed solution were sterilized separately and mixed afterward. The pH in the reactor was controlled at pH 6.7 with 25% NH_4OH. The temperature set-point was 37 °C. The dissolved oxygen concentration was controlled at 25% air saturation with a gas flow rate of 2 vvm sterile air, a system pressure of up to 2 bar, and stirrer speed (two 6 plate Rushton turbines).

Self-assembly and analysis of DNA origami structures. Staple oligonucleotides were purchased from Eurofins MWG, Ebersberg, Germany at HPSF grade. Assembly mixtures consisted of 20 nM scaffold ssDNA and 200 nM of each staple strand in a buffer containing 5 mM TRIS, 5 mM NaCl, 1 mM EDTA, and 20 mM $MgCl_2$ (pH 8). Reaction mixtures were subjected to a thermal annealing ramp in a TETRAD thermocycler (Bio-Rad Laboratories, Inc., Hercules, California, USA). For the single-layer rectangles, mixtures were heated to 65 °C for 15 min and then cooled from 65 to 60 °C in steps of 1 °C per 5 min and from 60 to 40 °C in steps of 1 °C per 30 s. For the multilayer structures, mixtures were heated to 65 °C for 15 min and then cooled from 60 to 40 °C in steps of 1 °C per 3 h. For negative-staining TEM samples were adsorbed on glow-discharged Formvar-supported carbon-coated Cu400 TEM grids (Science Services, Munich) and stained using a 2% aqueous uranyl formate solution containing 25 mM NaOH. Imaging was performed using a Philips CM100 EM operated at 100 kV. Images were acquired at 28 500-fold magnification using an AMT 4 Megapixel CCD camera.

■ ASSOCIATED CONTENT

Supporting Information

Host strain and phage variants, preculture preparation, feed profile equation, shake flask based fermentation, downstream processing, and analytics. The Supporting Information is available free of charge on the ACS Publications website at DOI: 10.1021/acs.nanolett.5b01461.

■ AUTHOR INFORMATION

Corresponding Author

*E-mail: d.weuster-botz@lrz.tum.de. Phone: ++49-89-289-15712. Fax: ++49-89-289-15714.

Notes

The authors declare no competing financial interest.

DOI: 10.1021/acs.nanolett.5b01461
Nano Lett. 2015, 15, 4672−4676

■ ACKNOWLEDGMENTS

We gratefully acknowledge the support in laboratory by Janina Edion (student TUM). We thank Thomas G. Martin for designing the rectangle variant and the 42-helix bundle and Matthias Schickinger for designing the gear object. This work was supported by Deutsche Forschungsgemeinschaft (DFG) through the TUM International Graduate School of Science and Engineering (IGSSE), the Excellence Cluster Center for Integrated Protein Science, Nano Initiative Munich, the Sonderforschungsbereich SFB863, and a European Research Council starting grant t256270 (to H.D.).

■ REFERENCES

(1) Rothemund, P. W. K. *Nature* **2006**, *440* (7082), 297−302 DOI: 10.1038/nature04586.
(2) Douglas, S. M.; Dietz, H.; Liedl, T.; Högberg, B.; Graf, F.; Shih, W. M. *Nature* **2009**, *459* (7245), 414−418 DOI: 10.1038/nature08016.
(3) Castro, C. E.; Kilchherr, F.; Kim, D.-N.; Shiao, E. L.; Wauer, T.; Wortmann, P.; Bathe, M.; Dietz, H. *Nat. Methods* **2011**, *8* (3), 221−229 DOI: 10.1038/nmeth.1570.
(4) Douglas, S. M.; Chou, J. J.; Shih, W. M. *Proc. Natl. Acad. Sci. U.S.A.* **2007**, *104* (16), 6644−6648 DOI: 10.1073/pnas.0700930104.
(5) Berardi, M. J.; Shih, W. M.; Harrison, S. C.; Chou, J. J. *Nature* **2011**, *476* (7358), 109−113 DOI: 10.1038/nature10257.
(6) Pfitzner, E.; Wachauf, C.; Kilchherr, F.; Pelz, B.; Shih, W. M.; Rief, M.; Dietz, H. *Angew. Chem., Int. Ed.* **2013**, *52* (30), 7766−7771 DOI: 10.1002/anie.201302727.
(7) Wei, R.; Martin, T. G.; Rant, U.; Dietz, H. *Angew. Chem., Int. Ed.* **2012**, *51* (20), 4864−4867 DOI: 10.1002/anie.201200688.
(8) Langecker, M.; Arnaut, V.; Martin, T. G.; List, J.; Renner, S.; Mayer, M.; Dietz, H.; Simmel, F. C. *Science* **2012**, *338* (6109), 932−936 DOI: 10.1126/science.1225624.
(9) Derr, N. D.; Goodman, B. S.; Jungmann, R.; Leschziner, A. E.; Shih, W. M.; Reck-Peterson, S. L. *Science* **2012**, *338* (6107), 662−665 DOI: 10.1126/science.1226734.
(10) Jungmann, R.; Steinhauer, C.; Scheible, M.; Kuzyk, A.; Tinnefeld, P.; Simmel, F. C. *Nano Lett.* **2010**, *10* (11), 4756−4761 DOI: 10.1021/nl103427w.
(11) Kopperger, E.; Pirzer, T.; Simmel, F. C. *Nano Lett.* **2015**, *15* (4), 2693−2699 DOI: 10.1021/acs.nanolett.5b00351.
(12) Kuzyk, A.; Schreiber, R.; Fan, Z.; Pardatscher, G.; Roller, E.-M.; Högele, A.; Simmel, F. C.; Govorov, A. O.; Liedl, T. *Nature* **2012**, *483* (7389), 311−314 DOI: 10.1038/nature10889.
(13) Shaw, A.; Lundin, V.; Petrova, E.; Fördős, F.; Benson, E.; Al-Amin, A.; Herland, A.; Blokzijl, A.; Högberg, B.; Teixeira, A. I. *Nat. Methods* **2014**, *11* (8), 841−846 DOI: 10.1038/nmeth.3025.
(14) Andersen, E. S.; Dong, M.; Nielsen, M. M.; Jahn, K.; Subramani, R.; Mamdouh, W.; Golas, M. M.; Sander, B.; Stark, H.; Oliveira, C. L. P.; Pedersen, J. S.; Birkedal, V.; Besenbacher, F.; Gothelf, K. V.; Kjems, J. *Nature* **2009**, *459* (7243), 73−76 DOI: 10.1038/nature07971.
(15) Douglas, S. M.; Bachelet, I.; Church, G. M. *Science* **2012**, *335* (6070), 831−834 DOI: 10.1126/science.1214081.
(16) Zhao, Y.-X.; Shaw, A.; Zeng, X.; Benson, E.; Nyström, A. M.; Högberg, B. *ACS Nano* **2012**, *6* (10), 8684−8691 DOI: 10.1021/nn3022662.
(17) Perrault, S. D.; Shih, W. M. *ACS Nano* **2014**, *8* (5), 5132−5140 DOI: 10.1021/nn5011914.
(18) Stahl, E.; Martin, T. G.; Praetorius, F.; Dietz, H. *Angew. Chem., Int. Ed.* **2014**, *53* (47), 12735−12740 DOI: 10.1002/anie.201405991.
(19) Linko, V.; Dietz, H. *Curr. Opin. Biotechnol.* **2013**, *24* (4), 555−561 DOI: 10.1016/j.copbio.2013.02.001.
(20) Sobczak, J.-P. J.; Martin, T. G.; Gerling, T.; Dietz, H. *Science* **2012**, *338* (6113), 1458−1461 DOI: 10.1126/science.1229919.
(21) Gyllensten, U. B.; Erlich, H. A. *Proc. Natl. Acad. Sci. U. S. A.* **1988**, *85* (20), 7652−7656.
(22) Hultman, T.; Ståhl, S.; Hornes, E.; Uhlén, M. *Nucleic Acids Res.* **1989**, *17* (13), 4937−4946.
(23) Kujau, M.; Wölfl, S. *Mol. Biotechnol* **1997**, *7* (3), 333−335 DOI: 10.1007/BF02740823.
(24) Little, J. W.; Lehman, I. R.; Kaiser, A. D. *J. Biol. Chem.* **1967**, *242* (4), 672−678.
(25) Walder, R. Y.; Hayes, J. R.; Walder, J. A. *Nucleic Acids Res.* **1993**, *21* (18), 4339−4343 DOI: 10.1093/nar/21.18.4339.
(26) Williams, K. P.; Bartel, D. P. *Nucleic Acids Res.* **1995**, *23* (20), 4220−4221.
(27) Ali, M. M.; Li, F.; Zhang, Z.; Zhang, K.; Kang, D.-K.; Ankrum, J. A.; Le, X. C.; Zhao, W. *Chem. Soc. Rev.* **2014**, *43* (10), 3324−3341 DOI: 10.1039/c3cs60439j.
(28) Ducani, C.; Kaul, C.; Moche, M.; Shih, W. M.; Högberg, B. *Nat. Methods* **2013**, *10* (7), 647−652 DOI: 10.1038/nmeth.2503.
(29) Ducani, C.; Bernardinelli, G.; Högberg, B. *Nucleic Acids Res.* **2014**, *42* (16), 10596−10604 DOI: 10.1093/nar/gku737.
(30) Nelissen, F. H. T.; Goossens, E. P. M.; Tessari, M.; Heus, H. A. *Anal. Biochem.* **2015**, DOI: 10.1016/j.ab.2015.01.014.
(31) Gu, H.; Breaker, R. R. *BioTechniques* **2013**, *54* (6), 337−343 DOI: 10.2144/000114009.
(32) Sambrook, J.; Fritsch, E. F.; Maniatis, T. *Molecular cloning. A laboratory manual*, 3rd ed.; Cold Spring Harbor Laboratory Press: Cold Spring Harbor, NY, 2001.
(33) Bellot, G.; McClintock, M. A.; Chou, J. J.; Shih, W. M. *Nat. Protoc* **2013**, *8* (4), 755−770 DOI: 10.1038/nprot.2013.037.
(34) Riesenberg, D.; Schulz, V.; Knorre, W. A.; Pohl, H. D.; Korz, D.; Sanders, E. A.; Roß, A.; Deckwer, W. D. *J. Biotechnol.* **1991**, *20* (1), 17−27 DOI: 10.1016/0168-1656(91)90032-Q.
(35) Korz, D.; Rinas, U.; Hellmuth, K.; Sanders, E.; Deckwer, W.-D. *J. Biotechnol.* **1995**, *39* (1), 59−65 DOI: 10.1016/0168-1656(94)00143-Z.
(36) Forsheit, A. B.; Ray, D. S.; Lica, L. *J. Mol. Biol.* **1971**, *57* (1), 117−127 DOI: 10.1016/0022-2836(71)90122-7.
(37) Warner, C.; Barker, N.; Lee, S.-W.; Perkins, E. *Bioprocess Biosyst Eng.* **2014**, 1−6 DOI: 10.1007/s00449-014-1184-7.
(38) Jung, S.-C.; Smith, C. L.; Lee, K.-S.; Hong, M.-E.; Kweon, D.-H.; Stephanopoulos, G.; Jin, Y.-S. *Appl. Environ. Microbiol.* **2010**, *76* (18), 6307−6309 DOI: 10.1128/AEM.01210-10.
(39) Grieco, S.-H.; Lee, S.; Dunbar, W. S.; MacGillivray, R. A.; Curtis, S. *Bioprocess Biosyst. Eng.* **2009**, *32* (6), 773−779 DOI: 10.1007/s00449-009-0303-3.
(40) Grieco, S.-H.; Wong, A. K.; Dunbar, W. S.; MacGillivray, R. A.; Curtis, S. *J. Ind. Microbiol. Biotechnol.* **2012**, *39* (10), 1515−1522 DOI: 10.1007/s10295-012-1148-3.
(41) Reddy, P.; McKenney, K. *Biotechniques* **1996**, *20* (5), 854−6 858, 860.
(42) Hofschneider, P. H. *Z. Naturforsch. B* **1963**, *18 b*, 203−210.
(43) Atha, D. H.; Ingham, K. C. *J. Biol. Chem.* **1981**, *256* (23), 12108−12117.
(44) Branston, S.; Stanley, E.; Keshavarz-Moore, E.; Ward, J. *Biotechnol. Prog.* **2012**, *28* (1), 129−136 DOI: 10.1002/btpr.705.
(45) Kim, D.-N.; Kilchherr, F.; Dietz, H.; Bathe, M. *Nucleic Acids Res.* **2012**, *40* (7), 2862−2868 DOI: 10.1093/nar/gkr1173.
(46) Bai, X.-C.; Martin, T. G.; Scheres, S. H. W.; Dietz, H. *Proc. Natl. Acad. Sci. U.S.A.* **2012**, *109* (49), 20012−20017 DOI: 10.1073/pnas.1215713109.
(47) Martin, T. G.; Dietz, H. *Nat. Commun.* **2012**, *3*, 1103 DOI: 10.1038/ncomms2095.

DOI: 10.1021/acs.nanolett.5b01461
Nano Lett. 2015, 15, 4672−4676